MJFAS
Malaysian Journal of Fundamental and Applied Sciences

Rohaizad *et al.* | Malaysian Journal of Fundamental and Applied Sciences, Vol. 22 (2026) 23–35

RESEARCH ARTICLE

Molecular Recognition in Imprinted Polymers for Selective Ibuprofen Adsorption: Influence of Monomer Selection and Monomer to Crosslinker Ratios

Nor Munirah Rohaizad[a,b], Suzylawati Ismail[a], Siew Chun Low[a,*]

[a]School of Chemical Engineering, Engineering Campus, Universiti Sains Malaysia, 14300 Nibong Tebal, Pulau Pinang, Malaysia; [b]Faculty of Chemical Engineering & Technology, Universiti Malaysia Perlis (UniMAP), 02600 Arau, Perlis, Malaysia

Abstract A computational study was conducted to simulate the pre-polymerization process of molecularly imprinted polymer (MIP) targeting ibuprofen (IBP), an extensively used non-steroidal anti-inflammatory drug. The study aimed to identify the most suitable functional monomer for IBP imprinting, evaluating the interactions of 2-vinyl pyridine (2VP), and methacrylic acid (MAA) with the IBP template molecule. Computational results indicated that MAA showed stronger hydrogen bonding and more favorable interactions with IBP compared to 2VP, making it a superior polymer for imprinting. Non-covalent imprinting was used to synthesize MIPs via the precipitation polymerization method. The synthesis was conducted by varying the key parameters, including the functional monomer types (2VP and MAA) and the molar ratio of template to functional monomers to crosslinker (1:4:20, 1:4:30 and 1:4:40). The resulting polymers, MIP-MAA and MIP-2VP, were characterized using fourier infra-red spectroscopy (FTIR) and field emission electron microscopy (FESEM). Binding efficiency was evaluated through batch rebinding assays. The results revealed that MIP-MAA exhibited significantly higher binding capacities and imprinting factors compared to MIP-2VP. Among the compositions tested, the MIP-MAA prepared with a 1:4:30 (MIP-MAA C30) demonstrated the best adsorption performance and the highest affinity toward IBP. This study emphasizes the potential of MIP-MAA as an efficient adsorbent for the selective extraction of IBP from environmental matrices, offering a promising solution for mitigating pharmaceutical pollution.

Keywords: Molecularly imprinted polymers, Ibuprofen, selective adsorption, molecular recognition.

Introduction

Globally, approximately 80% of wastewater and as much as 95% in some developing countries is discharged into the environment without undergoing treatment [1]. This untreated discharge introduces a diverse array of pollutants, including emerging contaminants (ECs) into aquatic ecosystems. ECs encompass anthropogenic organic compounds such as, synthetic hormones, pesticides, and pharmaceuticals, and personal care products (PPCPs). Among these non-steroidal anti-inflammatory drugs (NSAIDs) such as ibuprofen (IBP), diclofenac, and naproxen are among the most commonly detected due to their extensive usage and persistence, posing risks to environmental and human health.

IBP, also known by its chemical name 2-[4-(2-methylpropyl) phenyl] propanoic acid, is the third most consumed drug worldwide and widely prescribed for managing mild to moderate pain, inflammation, and fever [2]. Beyond its therapeutic use, IBP and its biologically active metabolites have been shown to negatively impact aquatic organisms [3]. It is frequently detected in wastewater treatment plants (WWTPs), hospital wastewaters, and sewage sludge, with concentrations reported as high as 95 μg L^{-1}, 208 ng g^{-1}, and 92 μg L^{-1}, respectively, across Europe, America, and Asia [4].

The selective adsorption of pharmaceutical compounds, particularly NSAIDs, has gained significant attention due to the persistence of these residues in natural water bodies and their associated

***For correspondence:**
chsclow@usm.my

Received: 22 Jan. 2025
Accepted: 13 August 2025

environmental risks. Effective removal strategies are crucial to addressing these threats. Among these, molecularly imprinted polymers (MIPs), emerge as a promising solution. MIPs are engineered materials designed for the selective binding of target molecules through polymerization. This process creates binding sites that match the template's shape and size, thus ensuring high specificity and selectivity. MIPs have demonstrated versatility across various fields, including analytical chemistry [5], [6], medicine [7], [8], environmental monitoring [9], [10], [11], and food safety [12], [13]. In the environmental context, MIPs are particularly effective for detecting and absorbing pollutants such as pesticides, heavy metals, and pharmaceuticals. Numerous literatures have emphasized the potential of MIPs for the removal of IBP from water [14], [15], [16], [17], underscoring their viability as a targeted approach for mitigating pharmaceutical pollution.

Imprinted polymers achieve molecular recognition through tailored chemical interplays between the imprint molecule and the polymer's functional groups. The effectiveness of imprinting largely depends on selecting an appropriate functional monomer, a process traditionally guided by trial-and-error procedure, which can be costly and time-consuming [18]. Computational modelling offers a transformative approach to this challenge, enabling a deeper understanding of molecular interactions and improving MIP design. Techniques such as molecular dynamics simulations, quantum mechanics, docking studies, free energy calculations, and machine learning can predict binding affinities, optimize polymer composition, and enhance the specificity and selectivity of MIPs. These advancements streamline material development, reduce cost, and support applications in environmental monitoring, drug delivery, and sensor technologies.

The performance of MIPs in selective adsorption is highly influenced by the precise selection and ratio of functional monomers to crosslinkers. Functional monomers establish specific interactions with the imprint molecule, creating imprinted cavities with tailored binding sites. Whereas, crosslinkers provide the structural integrity necessary for the stability of the polymer matrix. The ratio of these components is crucial, as it governs the adsorption capacity, specificity, and molecular recognition efficiency. An optimal ratio ensures that the imprinted cavities are well-defined and capable of selectively binding the target molecule, while preserving the thermal stability and mechanical of the MIP [19]. Investigating this ratio is essential for developing MIPs with enhanced performance, as an imbalance could lead to poor cavity formation, reduced selectivity, or compromised structural stability. Such studies enable the fine-tuning of MIP properties to suit specific applications in environmental monitoring, pharmaceuticals, and analytical chemistry.

Presently, this study focuses on developing MIPs for the selective removal of IBP from aqueous solution, combining molecular imprinting techniques with computational modelling. Computational screening is employed to identify functional monomers that exhibit strong binding interactions with the target molecule, offering insights into molecular recognition mechanisms. Additionally, the study evaluates the influence of varying functional monomer to crosslinker ratios on the adsorption capacity and selectivity of MIPs. The findings aim to optimize MIP design for the efficient removal of pharmaceutical contaminants from water systems.

Materials and Methods

The reagents used, include methacrylic acid (MAA), 2-vinylpyridine (2VP), ibuprofen (IBP), ethylene glycol dimethacrylate (EGDMA), and azobisisobutyronitrile (AIBN), all obtained from Sigma-Aldrich. Organic solvents such as ethanol (EtOH) and methanol (MeOH) were supplied by HmbG, while toluene and hydrochloric acid (HCl) were obtained from Merck.

Computational Modelling and Theoretical Calculation

Hyperchem 8.0 software (Hypercube, Inc.) was utilized for computational modelling to optimize polymer geometries. Using the semi-empirical PM3 quantum mechanics method, geometry optimization was performed on 2D-drawn templates and monomers, which were then converted to 3D structures. The interaction energy (ΔE_{int}) between the IBP and functional monomers was calculated using Eq. (1):

$$\Delta E_{int} = E_{complex} - E_{template} - E_{monomer} \quad (1)$$

This computational step aimed to predict the most suitable functional monomers for strong interaction with IBP. Validation of these results was carried out through synthesis and batch adsorption experiments.

Synthesis of MIP and NIP

MIPs and NIPs were synthesized using a precipitation polymerization method, modified from previous protocols [7]. Two types of monomers, 2VP and MAA, were tested at varying of the template to monomer to crosslinker molar ratios (1:4:20, 1:4:30 and 1:4:40) as tabulated in Table 1.

.

Table 1. Composition of the Pre-polymerization NIP and MIP based MAA and 2VP

Polymer	Template (mmol)	Monomer (mmol)		Crosslinker (mmol)
		MAA	2VP	
NIP-MAA	-	4	-	20, 30, 40
MIP-MAA	1	4	-	
NIP-2VP	-	-	4	
MIP-2VP	1	-	4	

For MIPs, IBP (template) was mixed with the chosen monomer in a reaction flask, followed by the addition of methanol (first porogen), and EGDMA (crosslinker). The mixture was sonicated for 5 minutes before AIBN (initiator) and toluene (second porogen) were added; followed by 10 minutes of additional sonication. The reaction mixture was magnetically stirred at 125 rpm in an oil bath at 65 °C for 24 hours after being purged with nitrogen gas for 10 minutes. NIPs were synthesized similarly, but without the template. The resulting polymers were crushed and ground into a fine powder. The IBP template was extracted using methanol with 0.1% 0.1 M HCl through multiple cycles of rotation and centrifugations (3500 rpm for 5 minutes). Template removal was confirmed using UV-Visible spectrophotometer (Agilent Cary 60) no longer detected the template. The template removed polymers were dried at 60 °C in an oven.

Characterization of NIP and MIP

The structure and surface properties of the polymers were analyzed using FTIR over the range of 4000–400 cm^{-1} (Vertex 70, Shimadzu, Kyoto, Japan) and FESEM (JSM-IT500). Porosity and surface area were assessed using Brunauer–Emmett–Teller (BET) theory, with degassing performed at 140 °C for 5 hours prior to analysis (Micromeritics ASAP-2020).

Binding Experiment

The binding performances of MIPs and NIPs were assessed to confirm the presence of selective cavities in MIPs. Stock IBP solutions in EtOH were prepared at concentrations of 10-100 mg/L. For each binding test, 25 mg of MIP was placed in a centrifuge tube with 10 ml of 50 mg/L IBP solution. The tubes were rotated at 40 rpm for 2 hours and centrifuged at 4000 rpm for 10 minutes. Residual IBP concentrations were measured using a UV-vis spectrophotometer at 230 nm. Adsorption capacity, Q (mg/g of polymer) was calculated using Eq. (2):

$$Q = \frac{C_0 - C_t}{W} \times V \quad (2)$$

where C_0 and C_t are the initial and final IBP concentrations (mg/L), V is the solution volume (L) and W is the polymer mass (g). The imprinting factor (IF) was calculated using Eq. (3):

$$IF = \frac{Q_{MIP}}{Q_{NIP}} \quad (3)$$

All experiments were conducted in triplicate for reproducibility.

Results and Discussion

Computational analysis of the pre-polymerization complex

IBP possesses reactive groups, such as -carboxyl (-COOH) group and an aromatic ring (Figure 1a), which facilitate hydrogen bonding interactions. MAA contributes a carboxyl group (single bond COOH) capable of forming strong hydrogen bonds with IBP's reactive sites. Specifically, the carbonyl oxygen of the carboxyl group in IBP acts as a hydrogen bond acceptor, forming bonds with the hydroxyl hydrogen of MAA (Figure 1b). MAA's dual role as a hydrogen bond donor and acceptor enhances its utility in creating stable molecular recognition sites during the polymerization process. In contrast, 2VP contains an amine group (-NH) and a nitrogen atom in the pyridine ring (Figure 1c), which interacts with IBP's carboxyl group. The lone pair of electrons on the nitrogen atom in 2VP acts as a hydrogen bond acceptor, binding to the proton on the -COOH group of IBP. This dual interaction capability underscores 2VP's potential for creating imprinted cavities tailored for IBP recognition.

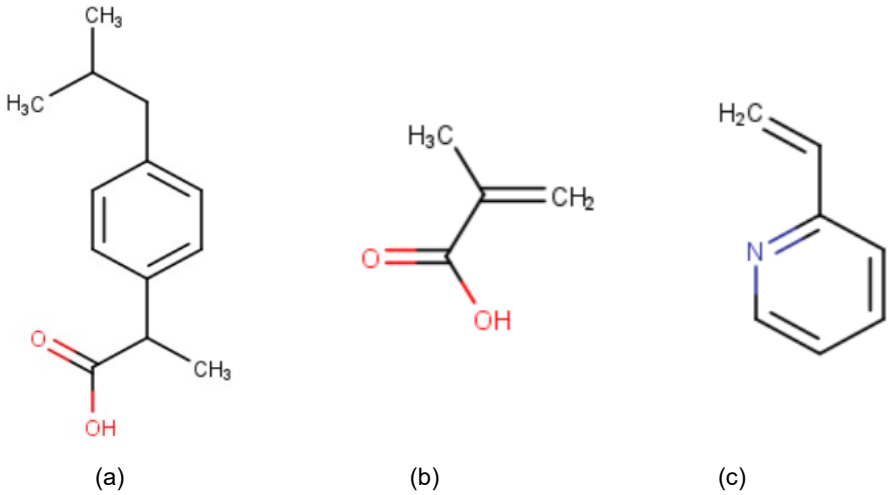

(a) (b) (c)

Figure 1. Chemical structure of (a) ibuprofen, (b) methacrylic acid and (c) 2-vinylpyridine (MarvinSketch 24.3.0, Chemaxon, 2024)

The efficiency of molecular recognition in imprinted polymers depends on the precise bonding interplays between the functional monomers and imprint molecules. Throughout the imprinting process, the functional groups of the template match those of the monomers, creating specific binding sites within the polymer matrix. Predicting the recognition mechanism of the imprinted polymer requires analyzing the pre-polymerization bonding interplays between the monomers and the imprint molecule [20]. The hydrogen bonding interactions and binding energies quantified in this study confirm the suitability of MAA and 2VP as functional monomers, each providing unique binding characteristics that influence the molecular recognition and adsorption performance of the resulting polymers. In fact, the binding interactions within the imprinted sites are primarily determined by the functional monomers, as their functional groups are specifically matched with those of the imprint molecule during the molecular imprinting process [21].

The selective mechanism of the IBP imprinted polymer was further elucidated using molecular simulations, supported by detailed atomic charge calculations for each atom in the functional monomer and template molecules. Semi-empirical PM3 computational methods were employed to determine bonding charges, as summarized in Table 2. These charges are used to identify atoms most likely involved in forming a hydrogen bond. The analysis revealed that H23 of IBP serves as a proton donor, meanwhile O6 of MAA acts as a proton acceptor, with a calculated hydrogen bond length of 1.56 Å Additionally, hydrogen bonding is observed where the oxygen atom of MAA acts as a proton acceptor, which interacting with the proton from the carboxylic group of IBP. Likewise, H9 of MAA was identified as a proton donor and interacting with O10 of IBP as a proton acceptor, forming a hydrogen bond of 1.59 Å. Quantitatively, the bond highlights the robustness of the monomer-template interaction, which provides insights into tailoring functional monomers for improved polymer performance.

Table 2. Bonding charges of IBP and MAA.

Bonding charges of IBP and MAA					
IBP			MAA		
Atom no.	Atom	Bonding charges (x10^{-2})	Atom no.	Atom	Bonding charges (x10^{-2})
1	C	-9.9	1	C	-7.6
2	C	-6.6	2	C	-14.3
3	C	-11.3	3	C	42.2
4	C	-8.3	4	O	-30.2
5	C	-10.2	5	C	-6.6
6	C	-1.2	**6**	**O**	**-40.5**
7	C	11.0	7	H	8.3
8	C	38.1	8	H	10.1

Bonding charges of IBP and MAA					
IBP			MAA		
Atom no.	Atom	Bonding charges (x10^{-2})	Atom no.	Atom	Bonding charges (x10^{-2})
9	O	-30.6	**9**	**H**	**22.8**
10	**O**	**-39.5**	10	H	6.4
11	C	-6.0	11	H	4.8
12	C	-7.2	12	H	4.8
13	C	-11.3			
14	C	-12.2			
15	C	-8.5		**2VP**	
16	H	10.9	1	C	-6.4
17	H	11.7	2	C	-16.4
18	H	10.6	3	C	-4.4
19	H	8.8	4	N	-6.6
20	H	4.6	5	C	-1.3
21	H	4.9	6	C	-14.4
22	H	5.9	7	C	-12.9
23	**H**	**22.5**	8	C	-11.3
24	H	5.8	9	H	10.6
25	H	6.1	10	H	11.2
26	H	6.9	11	H	11.7
27	H	4.1	12	H	11.5
28	H	4.0	13	H	10.5
29	H	3.9	14	H	7.6
30	H	4.2	15	H	10.6
31	H	4.1			
32	H	4.6			
33	H	12.2			

Figure 2 illustrates the optimized geometries of complexes and highlights potential hydrogen bonding interactions. Analysis reveals that IBP forms with MAA, confirming a strong intermolecular interaction. As mentioned earlier, the calculated hydrogen bond lengths are approximately 1.56 Å and 1.59 Å, involving the carboxylic and hydroxyl groups of IBP and MAA, respectively, contributing to the stability of the complex. In contrast, no hydrogen bonds were detected in the IBP-2VP complex, suggesting that 2VP relies on other types of chemical interactions, such as dipole or van der Waals forces, for binding.

The interaction energy measures the stability of the geometries formed between the IBP template molecule and various monomers, with lower interaction energies indicating increased stability. Binding energy (ΔE) is used as a quantitative indicator of hydrogen bonding strength, where more negative ΔE values represent stronger binding interactions. Molecular simulation calculations provided the binding energies for the bonding interplay between the functional monomer and IBP, with the results summarized in Table 3. The data revealed that both IBP-MAA and IBP-2VP complexes had negative binding energy values, signifying that their bindings were stabilized. With the lowest binding energy of -19.84 kcal/mol among the complexes examined, the IBP-MAA complex exhibited the most stable geometry. As seen in Figure 2a, this stability was ascribed to frequent hydrogen bonding between the carboxylic (-COOH) group of IBP and the acidic protons of MAA. Additionally, its improved binding affinity was further influenced by the potent acid-base interactions that existed between the acidic carboxylate group of IBP and the functional group of MAA. This binding energy aligns well with values reported for similar complexes [21], [22]. Conversely, the IBP-2VP complex had a binding energy of -13.85 kcal/mol, indicating comparatively weaker interactions.

The pyridine ring in 2VP formed van der Waals interactions, which lacked the strength of the hydrogen bonding observed in the IBP-MAA complex. Additionally, a stacking electrostatic interaction might occur between the aromatic rings of both the template and the functional monomer (pyridine group) [21].

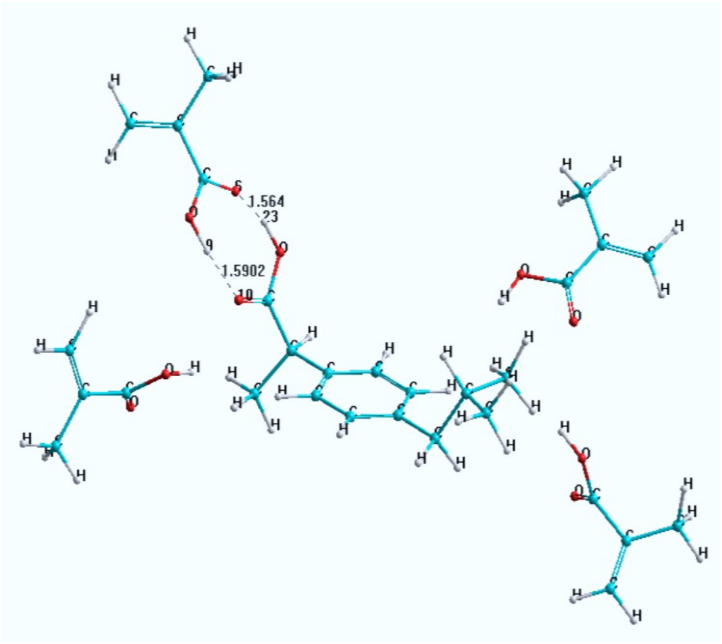

(a)

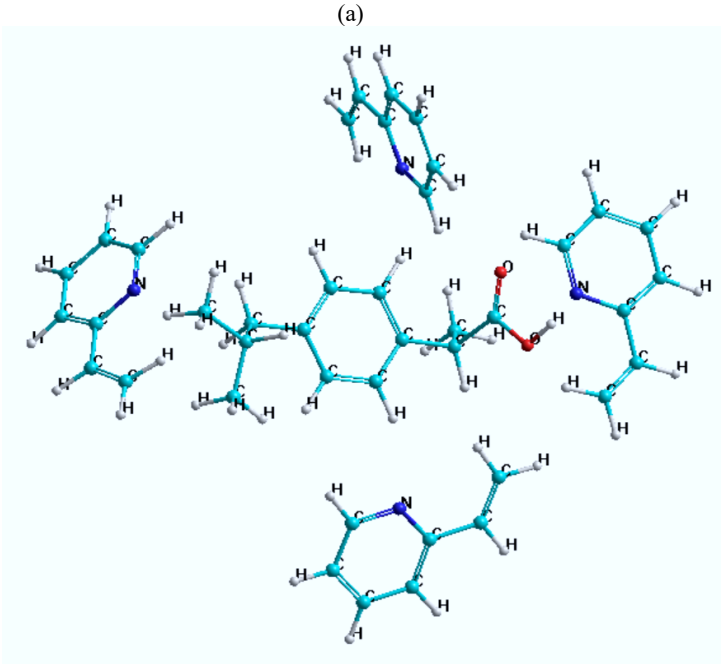

(b)

Figure 2. The optimized geometries of monomers with template molecule in a 1:4 ratio (a) interaction between MAA-IBP and (b) 2VP-IBP complexes. A black dash represents the hydrogen bond. (Color code: cyan = C atom, grey = H atom, red = O atom, blue = N atom)

Table 3. Binding energies ΔE of IBP with 2-vinylpyridine (2VP) and methacrylic acid (MAA) at a molar ratio of 1:4

Complexes	İnteraction energy, ΔE (kcal/mol)
IBP-2VP	-13.85
IBP-MAA	-19.84

The geometric configurations of these complexes, as shown in Figure 2, highlight the differences in the bonding mechanisms. MAA establishes dual hydrogen bonds with IBP, while 2VP fails to form any hydrogen bonds with IBP under the given conditions. The theoretical simulations also emphasized the critical role of hydrogen bonding in the rebinding ability of IBP-imprinted sites. Strong hydrogen bonds facilitated greater rebinding of the template molecule to the imprinted sites. In contrast, van der Waals interactions dominated the interactions between structural analogs of IBP and functional monomers, contributing to lower binding affinities. These simulation results aligned with selective binding experiments, further validating the superior selectivity of IBP-imprinted polymers. The data in Table 3 corroborate these findings by quantitatively illustrating the disparities in binding strengths among the tested complexes. MIPs and NIPs, formulated with molar ratios matching the simulated systems, underwent nitrogen sorption analysis to characterize their morphology and physical properties.

Characterization of NIP and MIP Functional Groups

The FTIR spectra for NIP and MIP derived from MAA and 2VP monomers are displayed in Figure 3. Both spectra exhibit similar bands at 3490 cm^{-1} (O-H stretching of the carboxyl group), 2979 cm^{-1} (C-H stretching of the carboxyl group), 1730 cm^{-1} (C═O bond), 1640 cm^{-1} (C═C bond stretching vibration), as well as 1470 cm^{-1} and 1387 cm^{-1} (CH_3, CH_2 deformations), reflecting the characteristic polymer's functional groups. The identical band shapes and positions indicate that both NIP and MIP share a similar backbone structure, suggesting complete template removal. The transmittance intensity is notably higher in MIP, such as the peak at 3490 cm^{-1}, indicating hydrogen bonding in the MIP. In 2VP-based MIPs, a distinctive peak at 1597 cm^{-1} corresponds to C=N stretching in the pyridine ring. Additionally, the adsorption band at 1465 cm^{-1} arises from C=C ring stretching. A shift in the carboxyl group's C=O stretching vibration from 1716 cm^{-1} to 1730 cm^{-1} further supports hydrogen bonding interactions between the OH groups of MAA or 2VP and the COOH group of IBP, aligning with previously reported findings [23]. These spectral changes emphasize the role of hydrogen bonding in stabilizing the MIP's selective interactions.

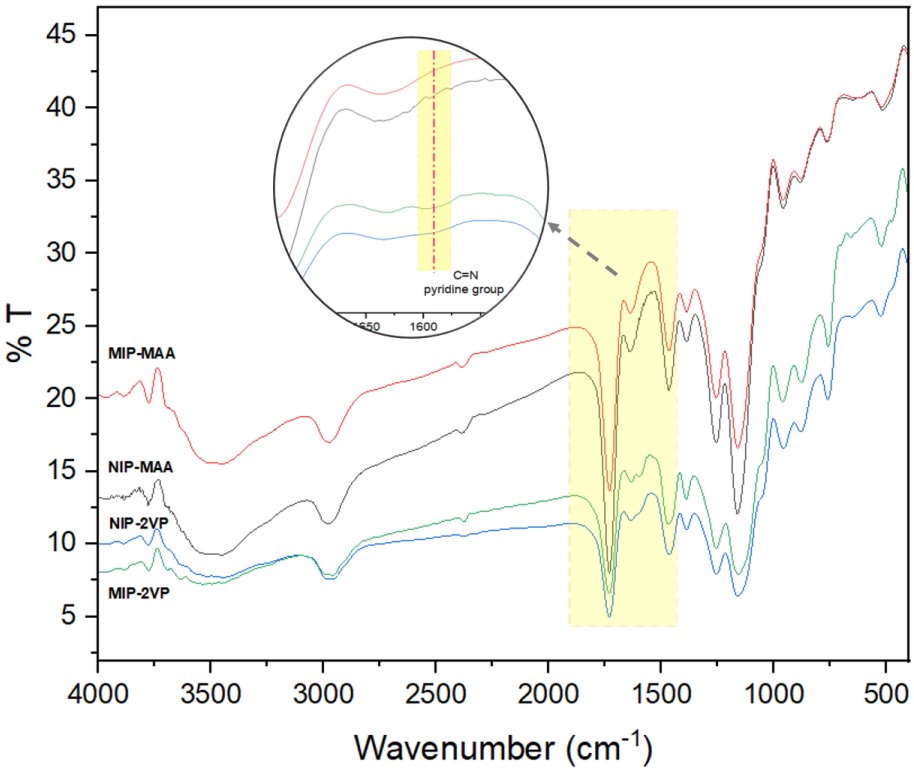

Figure 3. FTIR spectra of NIP and MIP based 2VP and MAA

Table 4 highlights two distinct bands, where a strong absorption at 1716 cm^{-1} is ascribed to carboxyl stretching of the isopropionic acid group, and another at 2941 cm^{-1}, is associated with hydroxyl stretching vibrations. Additionally, aromatic ring vibrations corresponding to C–C and C=C stretches are identified at 1508 cm^{-1} and 1423 cm^{-1}, respectively. The FTIR spectra of MAA- and 2VP-based MIPs reveal all these IBP-specific bands, confirming the drug's incorporation within the polymer matrix. This spectral evidence shows the successful inclusion of IBP functional groups during the imprinting process, with the characteristic vibrational modes serving as indicators of the drug's molecular structure within the MIP framework. The retention of these bands indicates stable interactions between IBP and the functional monomers during polymerization.

Table 4. Characteristic bands of IBP

Wavenumber (cm^{-1})	Functional group
2941	O-H Stretch (Carboxylic Acid)
1716	C=O Stretch (Carboxylic Acid)
1508	C-C stretch (Aromatic ring)
1423	C=C stretch (Aromatic ring)

Surface Area

As depicted in Table 5, the specific surface area and average pore diameter of MIP-MAA are 357.04 m^2/g and 15.64 nm, respectively, while those of NIP-MAA are 353.85 m^2/g and 15.09 nm, respectively. The slightly increased pore size and specific surface area of MIP-MAA suggest enhanced adsorption capacity, attributed to the effective distribution of binding sites within the imprinted cavities [14]. Comparatively, MIP-2VP has a pore diameter of 17.71 nm and surface area of 372 m^2/g; slightly surpassing the MAA-based counterparts [16].

Table 5. Textural properties of NIPs and MIPs

	BET Surface Area (m^2/g)	Average pore diameter (nm)	Reference
NIP-MAA	353.85	15.09	
MIP-MAA	357.04	15.64	
NIP-2VP	318	11.14	[16]
MIP-2VP	372	17.71	

Figure 4 illustrates the isotherms of adsorption and desorption for MIP-MAA exhibit a type II curve, which is indicative of nonporous or macroporous materials. The gradual curvature in the isotherm represents the coexistence of monolayer coverage and the initiation of multilayer adsorption, leading to pore condensation within mesopores. The desorption branch forms a narrow type H3 hysteresis loop, with the adsorption and desorption branches running parallel. The presence of an H3 loop signifies a pore network predominantly characterized by macropores that are not entirely filled with pore condensate.

Both MIP-MAA and NIP-MAA have pore diameters ranging from 2 to 50 nm, validating the formation of mesoporous polymers during the polymerization process. The pore formation is largely influenced by the choice of porogen, which, when combined, generates various pore types, including micropore-mesopore, mesopore-macropore or micropore-macropore [24]. The use of toluene and methanol as porogen mixture in this study facilitated the formation of a mixture of macropores and mesopores, as reflected in the pore size distribution (PSD) curve (see inset figure). The PSD reveals a broad, multimodal range extending from 4-80 nm, with the majority of pores distributed between 4-50 nm, corresponding to mesopores. Additionally, a significant presence of macropores was noted in the MIP-MAA, further enhancing its adsorption capacity and material utility in sensing specific target analytes.

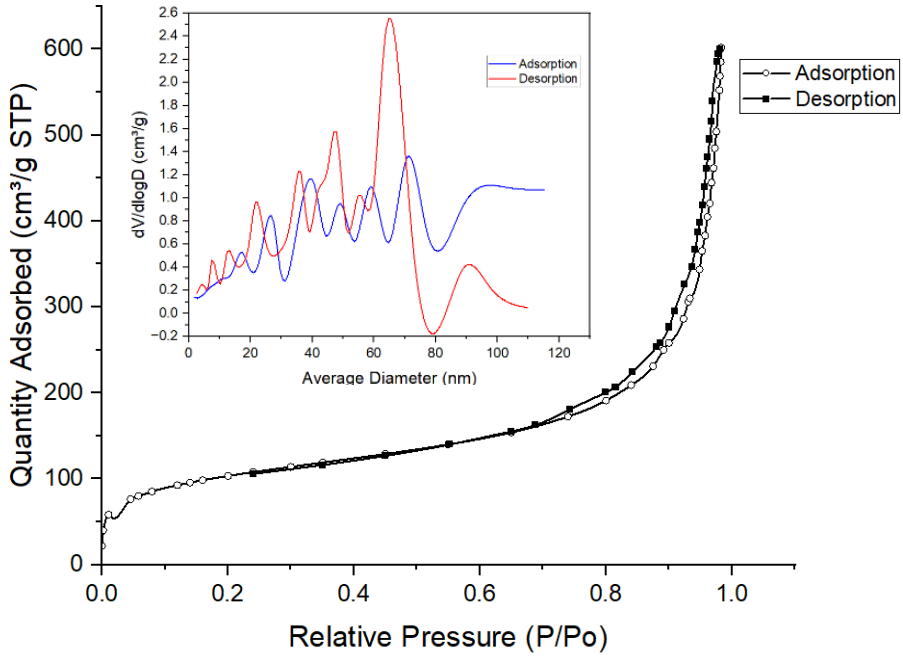

Figure 4. Adsorption and desorption curves of MIP-MAA and pore size distribution curves

Surface Morphology

The SEM images of NIP-MAA and MIP-MAA are depicted in Figure 5 (a) and (b), respectively. Significant differences are observed between the surface of NIP and MIP. Both materials exhibited irregular shapes with a monolithic particle appearance and porous surfaces indicative of high surface area. Notably, the MIP displays a rougher surface than the NIP, suggesting the existence of cavities developed on the MIP surface during the imprinting process. These cavities provide more binding sites for IBP adsorption and facilitate enhanced mass transfer into the pores. Additionally, the larger pore size in MIPs relative to NIPs further substantiates the imprinting effect, as it represents the formation of cavities tailored for improved adsorption performance. These structural features align with the observed enhancement in adsorption efficiency discussed later in Figure 6.

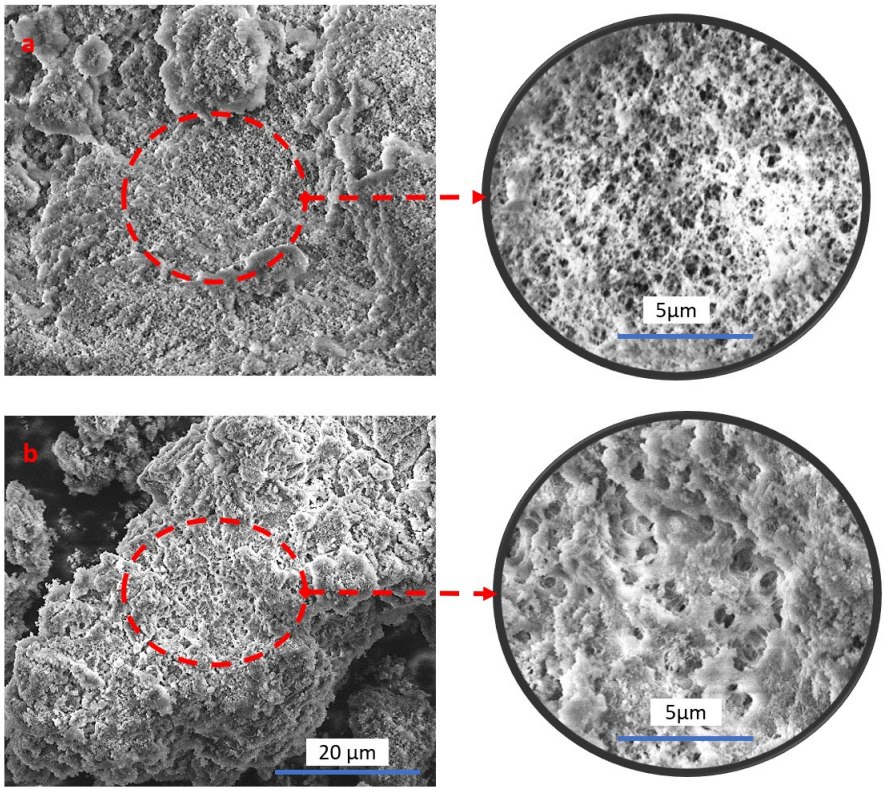

Figure 5. SEM micrographs of (a) NIP-MAA and (b) MIP-MAA

Binding Performance

İn this study, two functional monomers, MAA and 2VP, were used to identify the most effective monomer for interacting with IBP, aiming to enhance binding performance in terms of binding capacity and imprinting factor. The properties of the imprinted cavities are crucial in determining the effectiveness of MIPs compared to NIPs. The experimental results reveal a significant difference in adsorption performance between MIP-MAA and MIP-2VP. As expected, MIP-MAA exhibited higher binding capacity and imprinting factor than MIP-2VP. The experimental results will verify the reliability of the former theoretical simulation. The reason is more stable complex was formed with high interaction energy between IBP and MAA molecules, as reported previously. Therefore, the MIP-MAA complex would have a greater affinity than that of MIP-2VP during the rebinding test. These findings aligned with earlier studies where MIPs synthesized with MAA demonstrated superior performance in adsorbing NSAIDs like IBP. For instance, a study reported that MIPs prepared with MAA achieved a retention percentage of 98.3% for diclofenac, naproxen, and ibuprofen, indicating high binding affinity and selectivity [16].

The enhanced performance of MIP-MAA can be attributed to the formation of stable complexes with IBP, resulting from strong interactions between the carboxyl group of MAA and the functional groups of IBP. This interaction leads to the creation of specific binding sites within the polymer matrix, facilitating selective rebinding of the template molecule. In contrast, MIP-2VP, with its pyridine nitrogen, forms fewer stable complexes with IBP, resulting in lower binding capacity and imprinting factor. These findings highlight the importance of selecting appropriate functional monomers to achieve optimal binding performance in MIPs. The choice of monomer significantly influences the template–polymer complex's stability and the formation of specific cavities, thereby affecting the overall efficiency of the MIP in adsorbing target molecules.

When comparing different template: monomer: crosslinker (T:M:C) ratios, it was evident from Figure 6b that the adsorption capacity of MIP-MAA initially increased as the crosslinker ratio got higher before slightly decreasing. The maximum adsorption capacity was observed at a monomer: crosslinker molar ratio of 4:30 (MAA-C30).

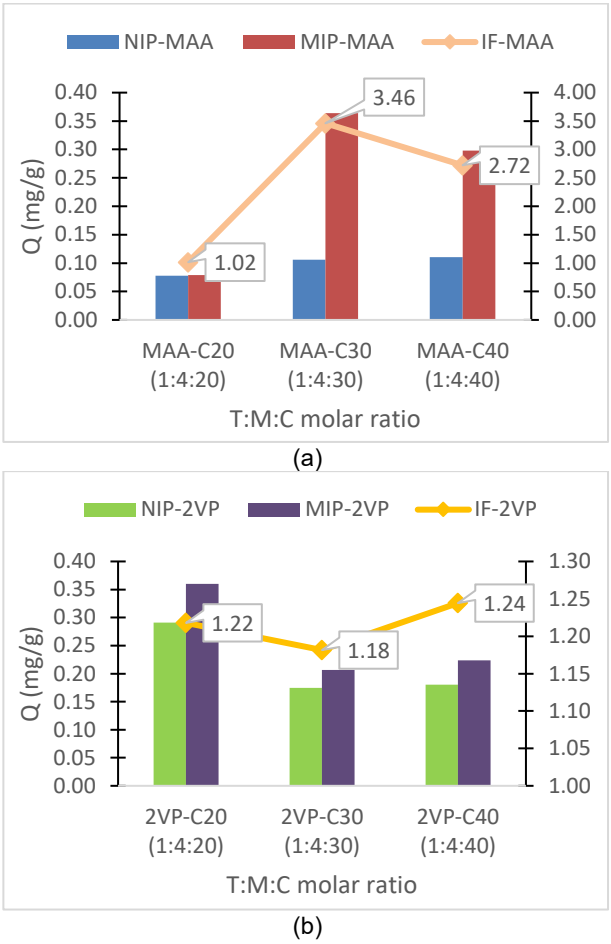

Figure 6. The adsorption capacity (Q) and imprinting factor (IF) of MIPs and NIPs for different type of monomer (a) MAA and (b) 2VP and T:M:C molar ratio

Specifically, MAA-C30 showed the highest binding capacity of 0.364 mg/g, with MAA-C40 and MAA-C20 following at 0.298 mg/g and 0.079 mg/g, respectively. The observed trend can be ascribed to the role of the crosslinker in enhancing the rigidity of the polymer matrix. An optimal crosslinker concentration improves the structural integrity and stability of the binding sites by preserving their specific shape and size. This structural reinforcement maximizes the retention of the template molecule within the cavity. Higher crosslinker amounts create a polymer network rigid enough to accommodate large template molecules and maintain efficient binding [19]. However, excessive crosslinker usage could result in overly rigid polymers that may hinder template accessibility to the binding cavities, thereby reducing adsorption capacity. Conversely, an insufficient crosslinker amount may fail to establish the three-dimensional cavity structure necessary for effective template recognition. Additionally, as illustrated in Figure 6, the binding capacity values of NIPs were relatively lower compared to those of MIPs. This disparity highlights the inability of NIPs to bind template molecules effectively due to the absence of specific cavities capable of template recognition [25]. This stark contrast indicates the critical importance of imprinting in the design of polymers for selective adsorption applications.

The binding capacity of MIP-2VP displayed a distinct trend, reaching its peak at a T:M:C ratio of 1:4:20 before gradually decreasing as the crosslinker amount increased. This decline can be attributed to the formation of an overly compact network caused by excessive cross-linking agents [25]. Such a dense network reduces the accessibility of binding sites, hindering the effective dispersion of MIP microspheres and thereby diminishing the adsorption capacity for targeted molecules.

Moreover, the IF for MIP-2VP polymers showed minimal variation across the different ratios, indicating that the crosslinker amount had a negligible impact on enhancing the binding affinity. This observation

suggests that although MIP-2VP possesses pores that provide binding sites, the shape and structure of these pores are not complementary to the template molecule, resulting in limited selective binding. In comparison MIP-MAA demonstrated superior performance, with the highest IF value identified at a T:M:C ratio of 1:4:30 (MAA-C30). This indicates that MAA-30 exhibited the strongest binding affinity to IBP, achieving optimal template recognition under these conditions. Specifically, MAA-C30 recorded an IF of 3.46, reflecting its exceptional ability to bind IBP in an effective and selective manner. Conversely, the IF values for MAA-C20 and MAA-C40 were lower, at 1.41 and 2.72, respectively, suggesting reduced binding affinity and less effective template recognition under these conditions. This highlights the critical influence of the T:M:C ratio in optimizing the performance of MIPs, particularly when using MAA as the functional monomer.

Conclusions

This study utilized computational simulations to examine the binding interactions between IBP and the functional monomers (MAA or 2VP), focusing on hydrogen bonding. The simulations identified MAA as the most suitable functional monomer for interacting with IBP, based on its superior binding affinity. The calculated binding energy for the IBP-MAA complex was determined to be -19.84 kcal/mol, indicating stronger binding interaction compared to IBP-2VP. This suggests that MAA forms a more stable and energetically favorable complex with IBP. These computational findings were corroborated by experimental results, which demonstrated that MAA-based MIPs exhibited the highest adsorption capacity for IBP. The adsorption performance of the MIPs was notably influenced by the concentration of the crosslinker agent, with optimal results achieved at higher crosslinker concentrations. Specifically, the most effective combination was found to involve 1:4:30 ratio of IBP to MAA to crosslinker, resulting in the most stable template-monomer complex and superior binding affinity toward IBP. This highlights the critical role of both the functional monomer and crosslinker concentration in optimizing the performance of MIPs for selective adsorption.

Conflicts of Interest

The authors declare that there is no conflict of interest regarding the publication of this paper.

Acknowledgment

This research was funded by the Ministry of Higher Education Malaysia (MoHE) Fundamental Research Grant Scheme (FRGS/1/2021/TK0/USM/02/8). The authors also acknowledge the financial support from Skim Latihan Akademik IPTA (SLAI) by MoHE, Malaysia and Universiti Malaysia Perlis, Malaysia.

References

[1] Kim, S., Chu, K. H., Al-Hamadani, Y. A. J., Park, C. M., Jang, M., Kim, D.-H., Yu, M., Heo, J., & Yoon, Y. (2018). Removal of contaminants of emerging concern by membranes in water and wastewater: A review. *Chemical Engineering Journal, 335*, 896–914. https://doi.org/10.1016/j.cej.2017.11.044.

[2] Chopra, S., & Kumar, D. (2020). Ibuprofen as an emerging organic contaminant in environment, distribution and remediation. *Heliyon, 6*(6), e04087. https://doi.org/10.1016/j.heliyon.2020.e04087.

[3] Grochowicz, M., Szajnecki, Ł., & Rogulska, M. (2022). Crosslinked 4-vinylpyridine monodisperse functional microspheres for sorption of ibuprofen and ketoprofen. *Polymers, 14*, 2080. https://doi.org/10.3390/polym14102080.

[4] Brillas, E. (2022). A critical review on ibuprofen removal from synthetic waters, natural waters, and real wastewaters by advanced oxidation processes. *Science of the Total Environment.*

[5] Suzziani Rosslan, A., *et al.* (2022). A review on molecularly imprinted polymer (MIP) for electrochemical sensor development. *Malaysian Journal of Fundamental and Applied Sciences, 18*, 283–294.

[6] Adumitrăchioaie, A., Tertiş, M., Cernat, A., Săndulescu, R., & Cristea, C. (2018). Electrochemical methods based on molecularly imprinted polymers for drug detection: A review. *Electroanalysis.* https://doi.org/10.1002/elan.201800117.

[7] El-Schich, Z., *et al.* (2020). Molecularly imprinted polymers in biological applications. *Future Science OA.*

[8] Ang, Q. Y., & Low, S. C. (2019). Feasibility study on molecularly imprinted assays for biomedical diagnostics. *Journal of Molecular Recognition.* https://doi.org/10.1002/jmr.2808.

[9] Azizi, A., & Bottaro, C. S. (2020). A critical review of molecularly imprinted polymers for the analysis of organic pollutants in environmental water samples. *Journal of Chromatography A, 1614*, 460603. https://doi.org/10.1016/j.chroma.2019.460603.

[10] Akhtar, J., Amin, N. A. S., & Shahzad, K. (2016). A review on removal of pharmaceuticals from water by adsorption. *Desalination and Water Treatment, 57*(27), 12842–12860. https://doi.org/10.1080/19443994.2015.1121466.
[11] Roland, R. M., Bhawani, S. A., & Ibrahim, M. N. M. (2023). Synthesis of molecularly imprinted polymer by precipitation polymerization for the removal of ametryn. *BMC Chemistry, 17*(1). https://doi.org/10.1186/s13065-023-00955-7.
[12] Cengiz, N., Guclu, G., Kelebek, H., Capanoglu, E., & Selli, S. (2022). Application of molecularly imprinted polymers for the detection of volatile and off-odor compounds in food matrices. *Journal of Agricultural and Food Chemistry.* https://doi.org/10.1021/acs.jafc.2c01566.
[13] Gao, M., *et al.* (2020). Recent advances and future trends in the detection of contaminants by molecularly imprinted polymers in food samples. *Frontiers in Chemistry.* https://doi.org/10.3389/fchem.2020.00450.
[14] Madikizela, L. M., & Chimuka, L. (2016). Synthesis, adsorption and selectivity studies of a polymer imprinted with naproxen, ibuprofen and diclofenac. *Journal of Environmental Chemical Engineering, 4*(4), 4029–4037. https://doi.org/10.1016/j.jece.2016.08.003.
[15] Olcer, Y. A., Demirkurt, M., Demir, M. M., & Eroglu, A. E. (2017). Development of molecularly imprinted polymers (MIPs) as a solid phase extraction sorbent for the determination of ibuprofen in water. *RSC Advances, 7.* https://doi.org/10.1039/C7RA03730B.
[16] Meléndez-Marmolejo, J., *et al.* (2022). Design and application of molecularly imprinted polymers for adsorption and environmental assessment of anti-inflammatory drugs in wastewater samples. *Environmental Science and Pollution Research, 29*, 45885–45902. https://doi.org/10.1007/s11356-022-18537-7.
[17] Pap, S., Taggart, M. A., Shearer, L., Li, Y., Radovic, S., & Turk Sekulic, M. (2021). Removal behaviour of NSAIDs from wastewater using a P-functionalised microporous carbon. *Chemosphere, 264.* https://doi.org/10.1016/j.chemosphere.2020.128420.
[18] Madikizela, L. M., Zunngu, S. S., Mlunguza, N. Y., Tavengwa, N. T., Mdluli, P. S., & Chimuka, L. (2018). Application of molecularly imprinted polymer designed for the selective extraction of ketoprofen from wastewater. *Water SA, 44*(3), 406–418. https://doi.org/10.4314/wsa.v44i3.12.
[19] Pratama, K. F., Erwanta, M., Manik, R., Rahayu, D., & Hasanah, A. N. (2020). Effect of the molecularly imprinted polymer component ratio on analytical performance. *Chemical & Pharmaceutical Bulletin, 68*(11), 1013–1024. https://doi.org/10.1248/cpb.c20-00303.
[20] Samah, N. A., Sánchez-Martín, M. J., Sebastián, R. M., Valiente, M., & López-Mesas, M. (2018). Molecularly imprinted polymer for the removal of diclofenac from water: Synthesis and characterization. *Science of the Total Environment, 631–632*, 1534–1543. https://doi.org/10.1016/j.scitotenv.2018.03.417.
[21] Madikizela, L. M., Mdluli, P. S., & Chimuka, L. (2016). Experimental and theoretical study of molecular interactions between 2-vinyl pyridine and acidic pharmaceuticals used as multi-template molecules in molecularly imprinted polymer. *Reactive and Functional Polymers, 103*, 33–43. https://doi.org/10.1016/j.reactfunctpolym.2016.03.006.
[22] Farrington, K., & Regan, F. (2007). Investigation of the nature of MIP recognition: The development and characterisation of a MIP for ibuprofen. *Biosensors and Bioelectronics, 22*(6), 1138–1146. https://doi.org/10.1016/j.bios.2006.08.023.
[23] Namazi, Z., *et al.* (2019). Facile synthesis and characterization of ibuprofen-mesoporous hydroxyapatite nanohybrid as a sustained drug delivery system. *Iranian Journal of Pharmaceutical Research, 18*(3), 1196–1211.
[24] Hasanah, A. N., Fauzi, D., Witka, B. Z., Rahayu, D., & Pratiwi, R. (2020). Molecularly imprinted polymer for ethylmorphine with methacrylic acid and acrylamide as functional polymer in butanol using two polymerization methods. *Mediterranean Journal of Chemistry, 10*(3), 277–288.
[25] Zhou, M., Hu, N., Shu, S., & Wang, M. (2015). Molecularly imprinted nanomicrospheres as matrix solid-phase dispersant combined with gas chromatography for determination of four phosphorothioate pesticides in carrot and yacon. *Journal of Analytical Methods in Chemistry, 2015*. https://doi.org/10.1155/2015/867815.